September 1990

Doubly differential detachment cross sections for fast H^-–rare-gas collisions

Chih-Ray Liu
University of Nebraska - Lincoln

Anthony F. Starace
University of Nebraska-Lincoln, astarace1@unl.edu

Doubly differential detachment cross sections for fast H^-–rare-gas collisions

Chih-Ray Liu*
Department of Physics and Astronomy, The University of Nebraska, Lincoln, Nebraska 68588-0111 and Institute of Atomic and Molecular Sciences, Academia Sinica, Taipei, Taiwan 10764, Republic of China

Anthony F. Starace
Department of Physics and Astronomy, The University of Nebraska, Lincoln, Nebraska 68588-0111
(Received 14 March 1990)

Detailed theoretical analyses are presented of the projectile-energy dependence as well as the target dependence of the electron-detachment collision processes, $H^- + T \rightarrow H(n=2) + T^* + e^-$. These analyses are illustrated by calculations of both projectile-frame and laboratory-frame doubly differential cross sections (DDCS's) for 0.5-, 1.0-, and 1.5-MeV H^- collisions with He targets and for 0.5-MeV H^- collisions with Ne, Ar, Kr, and Xe targets; in addition, we present laboratory frame DDCS's for 0.1-MeV H^- collisions with Xe targets. Comparisons with available experimental data are given.

I. INTRODUCTION

The cross section for fast H^- detachment collisions, particularly that differential in the energy and angle of the detached electron, has been shown to depend sensitively on the low-energy states of the fundamental H-e^- three-body system.[1,2] In particular, projectile detachment plus excitation has been shown[2] to be a major contributor to the equal-velocity peak in the detached-electron doubly differential cross section (DDCS) seen experimentally[3] at and near 0° in the laboratory for the case of 0.5 MeV H^- on He. In this work we extend our analysis of the DDCS's for fast H^- detachment collisions by examining their dependence on the incident projectile energy as well as on the target atom.

Specifically we present here calculations of the DDCS's for the following detachment processes:

$$H^- + T \rightarrow H(1s) + T^* + e^- , \tag{1}$$

$$H^- + T \rightarrow H(n=2) + T^* + e^- . \tag{2}$$

In Eqs. (1) and (2) the symbol T indicates the target atom; on the right-hand side, the asterisk on T indicates that the target may be either in an excited state, bound or continuum, or in the unexcited ground state. In Sec. II we present the Born approximation formulas for the DDCS's for processes (1) and (2). In Sec. III we examine the dependence of these DDCS's on the incident projectile energy, and we present specific results for processes (1) and (2) for 0.5-, 1.0-, and 1.5-MeV H^- projectiles on He atom targets. For electrons detached at 0.7° in the laboratory frame, we compare our calculated laboratory-frame DDCS's with the experimental measurements of Menendez and Duncan given in Ref. 4. In Sec. IV we examine the dependence of these DDCS's on the target atom, and we present DDCS's for processes (1) and (2) for 0.5-MeV H^- projectiles on He, Ne, Ar, Kr, and Xe target atoms. In addition, we compare our laboratory-frame DDCS's for 0.5-MeV H^- on Ar with the experimental measurements of Duncan and Menendez[5] and our laboratory-frame DDCS's for 0.1-MeV H^- on Xe with experimental measurements of Andersen, Bangsgaard, and Sørensen.[6] Finally, we discuss our results and present some conclusions in Sec. V.

II. FIRST-ORDER BORN EXPRESSION FOR THE DDCS

For the case of He targets, detailed theoretical descriptions of our calculational procedures for the DDCS's for processes (1) and (2) have been presented elsewhere.[1,2,7,8] Here, therefore, we restrict ourselves to presenting the first-order Born approximation result for the DDCS for processes (1) and (2). The Born approximation result for the DDCS for electron detachment following collision of the projectile ion H^- with a target atom of atomic number Z may be expressed in terms of the atomic form factor $\epsilon_{00}^Z(K)$ and the incoherent-scattering function $S_{\rm inc}^Z(K)$ for the target as[9]

$$\frac{d\sigma}{d\omega dE} = k\Sigma_{nl}^G(k_P,\theta_P) , \tag{3}$$

where

$$\begin{aligned}\Sigma_{nl}^G(k_P,\theta_P) &= \frac{8\pi}{v_i^2}\int_{K_{\rm min}^n(0)}^{K_{\rm max}^n(0)} J_{nl}(K,k_P,\theta_P)|\epsilon_{00}^Z(K)-Z|^2\frac{1}{K^3}dK \\ &+ \frac{8\pi}{v_i^2}\int_{K_{\rm min}^n(\bar{I}_Z)}^{K_{\rm max}^n(\bar{I}_Z)} J_{nl}(K,k_P,\theta_P)S_{\rm inc}^Z(K)\frac{1}{K^3}dK .\end{aligned} \tag{4}$$

In Eq. (3), k is the momentum, $d\omega$ is the solid angle, and E is the energy of the detached electron in any convenient inertial reference frame. $\Sigma_{nl}^G(k_P,\theta_P)$ is a Galilean-invariant cross section[10] calculated in the center-of-mass frame and is dependent on the detached

electron's momentum k_P relative to the H atom, as well as on the angle θ_P that $\mathbf{k}_P$ makes with the axis defined by the incident projectile (P); nl denotes the final state of the H atom. $\Sigma^G_{nl}(k_P,\theta_P)$ is defined by Eq. (4), where v_i is the relative velocity of the projectile with respect to the target; $\mathbf{K}$ is the momentum transfer:

$$\mathbf{K}=\mathbf{k}_i-\mathbf{k}_f \ , \tag{5}$$

where $\mathbf{k}_i$ and $\mathbf{k}_f$ are the initial and final momenta of the projectile in the center-of-mass frame; $K^n_{\min}(0)$ and $K^n_{\max}(0)$ are the appropriate minimum and maximum values for the momentum transfer for the case in which the target remains unexcited, while $\bar{I}_Z$ in $K^n_{\min}(\bar{I}_Z)$ and $K^n_{\max}(\bar{I}_Z)$ implies that these latter are computed for some appropriate average excitation energy $\bar{I}_Z$ for the target. Specifically,

$$K^n_{\min}(0)=\frac{I_{\mathrm{H}^-}+\frac{k_P^2}{2}+\Delta_n}{v_i} \ , \tag{6}$$

$$K^n_{\min}(\bar{I}_Z)=\frac{I_{\mathrm{H}^-}+\bar{I}_Z+\frac{k_P^2}{2}+\Delta_n}{v_i} \ , \tag{7}$$

where I_{H^-} is the binding energy of the H^- ion (0.027751 a.u.), $\frac{1}{2}k_P^2$ is the kinetic energy of the detached electron in the projectile frame, and Δ_n is the excitation energy of the nth level of H above the H($1s$) ground-state energy. The use of $\bar{I}_Z$ and the closure approximation substitutes for an explicit summation over each of the excited states of the target.[11]

In this paper we have employed the explicit values for the atomic form factors and the incoherent-scattering functions given by Hubbell *et al.*[12] Finally, the function $J_{nl}(K,k_P,\theta_P)$ is defined by

$$J_{nl}(K,k_P,\theta_P)=\frac{1}{2\pi}\int_0^{2\pi}\sum_m |\epsilon^{\mathrm{H}^-}_{nlm}(\mathbf{K},\mathbf{k}_P)|^2 d\phi \ . \tag{8}$$

In Eq. (8) the transition form factor is defined by

$$\epsilon^{\mathrm{H}^-}_{nlm}(\mathbf{K},\mathbf{k}_P)\equiv\left\langle \psi^-_{nlm\mathbf{k}_P}\left|\sum_{i=1}^{2}\exp(i\mathbf{K}\cdot\mathbf{r}_i)\right|\psi_0\right\rangle \tag{9}$$

and corresponds to a transition from the ground state of H^- to the final state of the H-e^- system, in which the electron is detached with momentum $\mathbf{k}_P$ relative to the H atom and the H atom is left in the state H(nlm). The ground state of H^- is described by the wave function ψ_0, and the final state of the H-e^- system is described by the wave function $\psi^-_{nlm\mathbf{k}_P}$, where the minus superscript indicates that it satisfies incoming-wave boundary conditions. Equation (8) contains a summation over the magnetic sublevels of the H(nl) state, as well as an integration over the azimuthal angle ϕ of the scattered projectile in the center-of-mass frame. This latter integration makes J_{nl} independent of the azimuthal angle ϕ_P of the detached electron.

The DDCS in any convenient inertial reference frame is expressed in Eq. (3) in terms of the Galilean-invariant DDCS $\Sigma^G_{nl}(k_P,\theta_P)$, which is calculated according to Eq. (4) in the center-of-mass frame. In particular, the laboratory (L) -frame DDCS is given by

$$\left[\frac{d\sigma}{d\omega dE}\right]_L=k_L\Sigma^G_{nl}(k_P(k_L,\theta_L),\theta_P(k_L,\theta_L)) \ , \tag{10}$$

where k_L and θ_L are the magnitude and polar angle of the detached electron's momentum in the laboratory, and where k_P and θ_P are expressed as functions of k_L and θ_L. For fast H^- projectiles, the so-called projectile reference frame[10,13] is approximately an inertial reference frame.[14] In this approximation one may write

$$\mathbf{k}_L=\mathbf{v}_i+\mathbf{k}_P \ . \tag{11}$$

Furthermore, one may then define a projectile (P) -frame DDCS as[10,13]

$$\left[\frac{d\sigma}{d\omega dE}\right]_P=k_P\Sigma^G_{nl}(k_P,\theta_P) \ . \tag{12}$$

The low-energy dynamics of the H-e^- system is clearly exhibited in the projectile-frame DDCS in Eq. (12), and the simple relation (11) facilitates the subsequent interpretation of the laboratory-frame DDCS defined in Eq. (10).

The calculation of the H^- transition form factor, defined in Eq. (9), and of the function J_{nl} defined in Eq. (8), are discussed in detail in Refs. 2 and 7. The procedures described in these references are employed in the present calculations.[8] In particular, we have employed an adiabatic hyperspherical[15–17] representation for both the initial- and final-state wave functions of the H-e^- system. For the low-energy states of the H-e^- system in the projectile frame that are important for the description of the H^--detachment collisions considered here, the adiabatic hyperspherical approximation has proved to be highly effective in representing the relevant three-body correlation effects.[1,2,7]

III. PROJECTILE ENERGY DEPENDENCE OF THE DDCS

We examine here the projectile-energy dependence of the process,

$$\mathrm{H}^-+\mathrm{He}\rightarrow\mathrm{H}(n=1,2)+\mathrm{He}^*+e^- \ , \tag{13}$$

for incident H^- energies of 0.5, 1.0, and 1.5 MeV. We have selected this process since the experimental data of Menendez and Duncan[4] exist for these incident projectile energies for the related process,

$$\mathrm{H}^-+\mathrm{He}\rightarrow\mathrm{H}^*+\mathrm{He}^*+e^- \ . \tag{14}$$

That is, the experimental data[4] include all final states of excitation of the H atom. The experimental measurements were made for electrons detached at 0.7° in the laboratory.

Our calculated laboratory-frame DDCS's, as well as the experimentally measured DDCS's, are shown in Fig. 1. In order to compare the DDCS's for different H^- projectile energies conveniently, we plot the results versus

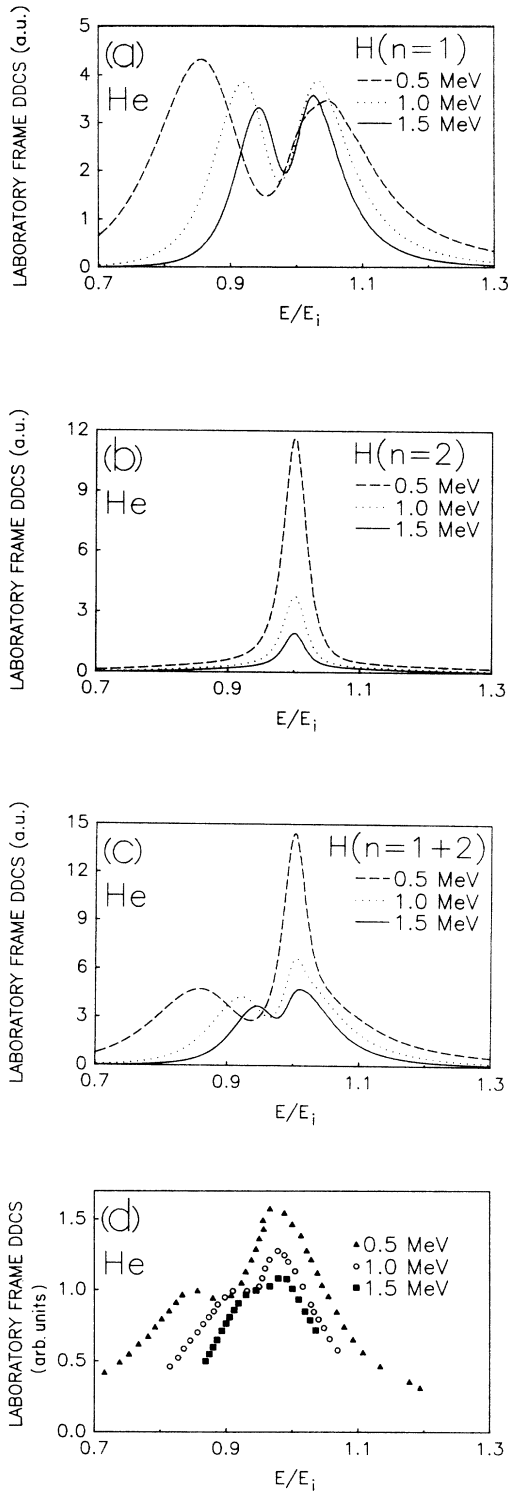

FIG. 1. Laboratory-frame DDCS's for $H^- + He \rightarrow H^* + He^* + e^-$ for detached electrons detected in the laboratory at 0.7° with respect to the incident H^- beam direction and for 0.5-MeV, 1.0-MeV, and 1.5-MeV H^- projectile energies. (a) Present calculated DDCS's for H($1s$) final states. (b) Present calculated DDCS's for H($n=2$) final states. (c) Sum of present calculated results for H($1s$) and H($n=2$) final states. (d) Experimental results of Macek, Menendez, and Duncan for all possible H final states (from Ref. 4).

the ratio of the detached-electron kinetic energy E to the kinetic energy E_i, at which the detached electron has the same velocity as the projectile (i.e., zero kinetic energy in the projectile frame), as is done in Ref. 4. Figure 1(a) shows our calculated laboratory-frame DDCS for the part of process (13) in which the H atom is left in the $n=1$ state. We see that the magnitudes of the DDCS's are not sensitive to the projectile energy in the energy range 0.5–1.5 MeV. We see also in Fig. 1(a) that the magnitude of the interference "window" in the DDCS in the laboratory frame is decreasing with increasing projectile energy.

Figure 1(b) shows our calculated laboratory-frame DDCS for the part of process (13) in which the H atom is left in the $n=2$ state. Clearly, there is a rapid decrease of this equal-velocity peak with increasing projectile energy. Figure 1(c) shows the sum of our results in Figs. 1(a) and 1(b) for comparison with the experimental data[4] for process (14), shown in Fig. 1(d). Comparison of Figs. 1(c) and 1(d) shows qualitative agreement of theory and experiment, indicating that excited states of H with $n>2$ are not significant contributors to process (14) in comparison with the H($1s$) and H($n=2$) states, at least for $\theta_L = 0.7°$.

The laboratory-frame theoretical and experimental data in Fig. 1 may be understood by an examination of the DDCS's for processes (1) and (2) in the projectile frame together with an analysis of the kinematic transformation from the projectile to the laboratory frame. The kinematics embodied in Eq. (11) that is relevant for electrons detached at 0.7° in the laboratory frame is shown graphically in Fig. 2. Figure 2 shows the locus of points θ_P ($k_L, \theta_L = 0.7°$) and k_P ($k_L, \theta_L = 0.7°$) traced out counterclockwise in the θ_P-k_P plane as k_L increases from small to large values. Two features of Fig. 2 should be noted. First, as the incident projectile energy increases, the minimum value of k_P increases. Second, as the incident projectile energy increases, the two allowed values of θ_P for a fixed value of k_P become closer together.

While the kinematics of the transformation from the projectile to the laboratory frame determines which parts of the projectile-frame DDCS contribute to the laboratory-frame DDCS, the DDCS's themselves depend

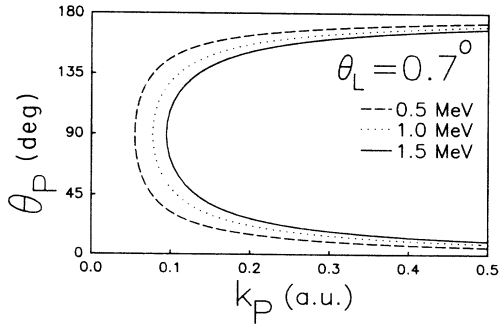

FIG. 2. Trajectories relating laboratory-frame electron momenta $\mathbf{k}_L \equiv (k_L, \theta_L = 0.7°)$ to projectile-frame electron momenta $\mathbf{k}_P \equiv (k_P, \theta_P)$ according to Eq. (11) for the three incident projectile energies, 0.5, 1.0, and 1.5 MeV.

on the incident projectile energy. From Eq. (4) we see that the Galilean-invariant DDCS depends inversely on the incident projectile energy. This dependence is compensated, however, by a decrease of $K^n_{\min}$ with increasing projectile velocity [cf. Eqs. (6) and (7)]. This decrease of $K^n_{\min}$ leads to a significant increase in the value of the integral in Eq. (4) for the invariant DDCS since the integrand is largest for small values of K. For the processes of interest in this work, only small values of k_P are of interest. Thus, from Eq. (11), k_L is almost proportional to the incident projectile velocity, which therefore affects the laboratory-frame DDCS's dependence on the projectile energy. In conclusion then, Eq. (12) shows that the projectile-frame DDCS, like the Galilean-invariant DDCS, has a factor v_i^{-2} dependence on the projectile velocity, which is compensated by the proportionality of $K^n_{\min}$ to v_i^{-1}. The laboratory-frame DDCS defined in Eq. (10), on the other hand, has a factor $k_L/v_i^2 \approx v_i^{-1}$ dependence on the projectile velocity, which is also compensated by the proportionality of $K^n_{\min}$ to v_i^{-1}.

With these observations on the kinematics in mind, consider now the DDCS's for processes (1) and (2) in the projectile frame, which are shown in Figs. 3 and 4, respectively. In Fig. 3 we show the Galilean-invariant DDCS [cf. Eq. (4)] for process (1). The valley extending from $k_P \approx 0$, $\theta_P \approx 0°$, out to $k_P = 0.5$ a.u., $\theta_P \approx 140°$, is due to an interference between the s- and p-waves of the outgoing, detached electron.[7,10,18] This valley causes the tra-

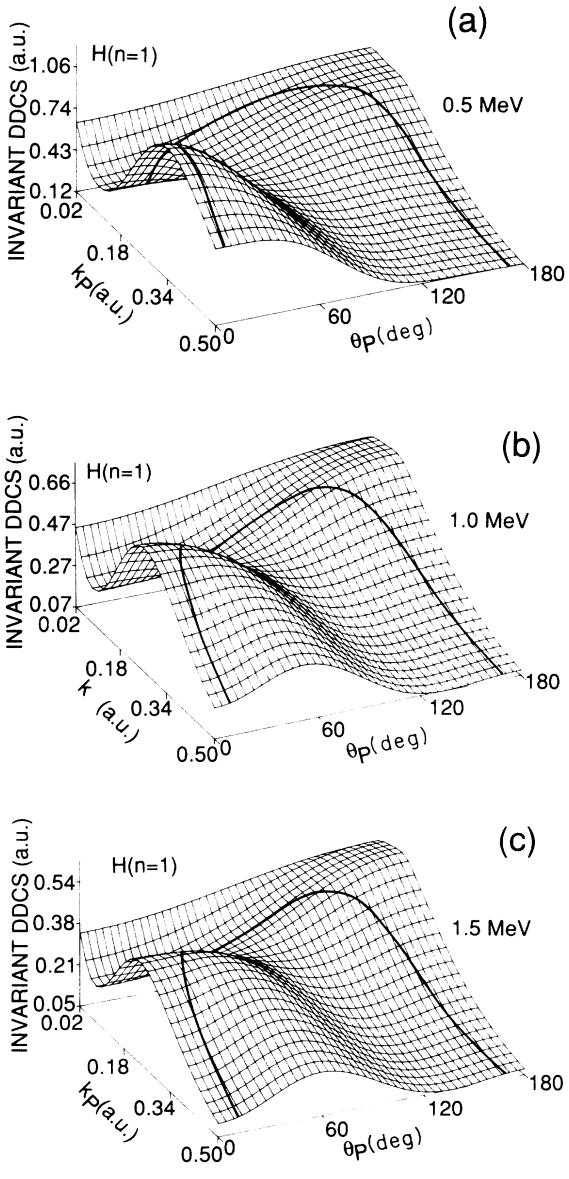

FIG. 3. Galilean-invariant DDCS's for process (1) for He targets plotted vs $\mathbf{k}_P \equiv (k_P, \theta_P)$. The solid-line trajectory on each surface maps the locus of points $\mathbf{k}_L \equiv (k_L, \theta_L = 0.7°)$ that contribute to the laboratory-frame DDCS's for $\theta_L = 0.7°$ [cf. Fig. 1(a)]. (a)–(c) Results for three values of the incident H^- energy, 0.5, 1.0, and 1.5 MeV, respectively.

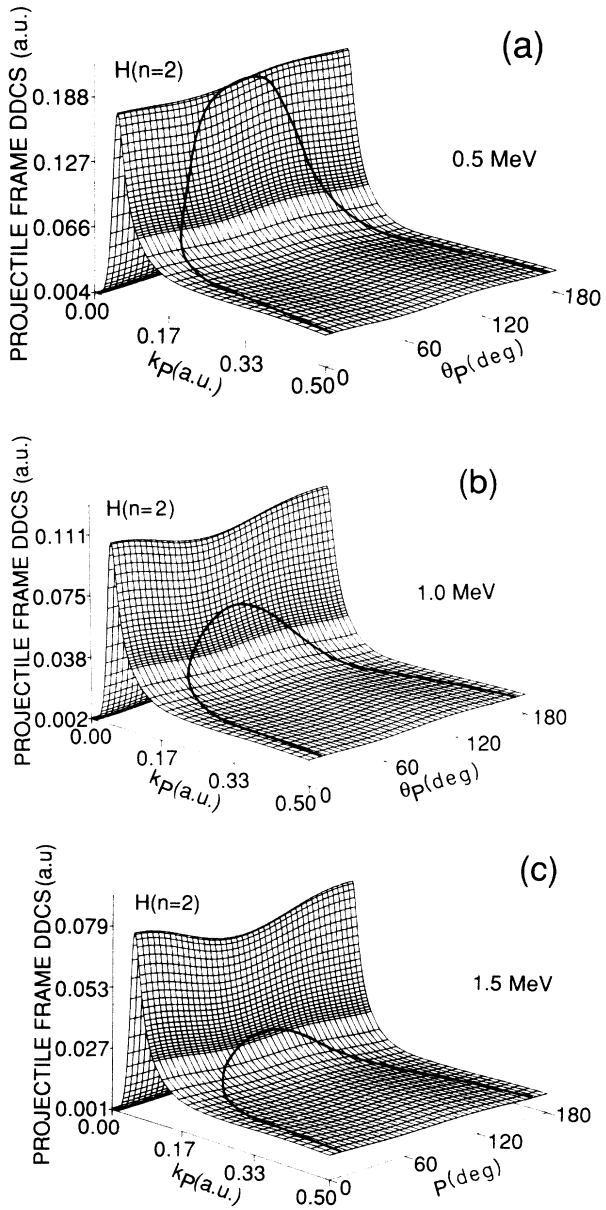

FIG. 4. Projectile-frame DDCS's for process (2) for He targets plotted vs $\mathbf{k}_P \equiv (k_P, \theta_P)$. The solid-line trajectory on each surface is defined in the caption for Fig. 3. (a)–(c) Results for three values of the incident H^- energy, 0.5, 1.0, and 1.5 MeV, respectively.

jectory for $\theta_L = 0.7°$ to have two maxima, which is the origin of the double-peaked structure of the laboratory-frame DDCS shown in Fig. 1(a). As the incident projectile energy increases, $k_P^{\min}$ increases and the spread of the $\theta_L = 0.7°$ trajectory in θ_P decreases, leading to a reduction of the minimum value of the $\theta_L = 0.7°$ trajectory, as seen in Fig. 1(a) in the laboratory frame. While the magnitudes of the Galilean-invariant DDCS's shown in Fig. 3 are decreasing with increasing v_i, the laboratory-frame DDCS's shown in Fig. 1(a) are relatively insensitive to the changes in v_i for the projectile energies from 0.5 to 1.5 MeV.

In Fig. 4 we show the projectile-frame DDCS's for process (2). The increasing value of $k_P^{\min}$ as the projectile energy increases causes the $\theta_L = 0.7°$ trajectory to lie increasingly far from the $^1P°$-shape resonance peak[1,2] at small values of k_P. It is this effect, which leads to the rapid decrease of the laboratory-frame DDCS's with increasing projectile energy, that is shown in Fig. 1(b).[19] The magnitude of the $^1P°$-shape resonance peak in the projectile-frame DDCS decreases with increasing projectile energy, but this decrease is reduced in the laboratory frame because of the multiplicative factor $k_L \approx v_i$ [cf. Eq. (10)].

IV. TARGET DEPENDENCE OF THE DDCS

The H^- detachment processes (1) and (2) depend on the target in several ways. As shown in Eq. (4), the Galilean-invariant DDCS depends on the target through the atomic form factor $\epsilon_{00}^Z(K)$, its atomic number Z, its incoherent scattering function $S_{\rm inc}^Z(K)$, and its average excitation energy $\bar{I}_Z$. In our calculations we have chosen $\bar{I}_Z$ for $Z=2$ to have that value (for small angles θ_L) for which the lower energy peak in the laboratory-frame DDCS for the H($1s$) final state lies at the same energy as found experimentally (cf. Fig. 1), as was done in our earlier works.[1,2,7] For each of the heavier rare gases, however, we have chosen $\bar{I}_Z$ to equal the excitation energy from the ground state to the energy location of the near-threshold peak in the photoionization cross section.[20] These values for $\bar{I}_Z$ are given in Table I together with the minimum values for the momentum transfers $K_{\min}^n(\bar{I}_Z)$ [cf. Eq. (7)] for 0.5-MeV H^- incident projectiles. We expect these ad hoc choices for $\bar{I}_Z$ to be reasonable for the small electron-detachment angles that are relevant here.

TABLE I. Average target excitation energies, $\bar{I}_Z$, and minimum momentum transfers, $K_{\min}^n(\bar{I}_Z)$, for H($n=1$) and H($n=2$) final states.

Z	$\bar{I}_Z$ (eV)	$K_{\min}^{n=1}(\bar{I}_Z)$ (a.u.)[a]	$K_{\min}^{n=2}(\bar{I}_Z)$ (a.u.)[a]
2	35.0	0.294	0.378
10	32.6	0.274	0.358
18	21.4	0.181	0.266
36	16.2	0.139	0.223
54	13.4	0.117	0.200

[a] $K_{\min}^n(\bar{I}_Z)$ is defined in Eq. (7). For this table we have set in Eq. (7) $k_P = 0$ and $v_i = 4.47135$ a.u. (corresponding to incident H^- projectiles having an energy of 0.5 MeV).

A detailed discussion of the sensitivity of the DDCS's to the choice of $\bar{I}_Z$ has been given in Sec. IV B of Ref. 2 for the case of He targets. In brief, when the H atom is left in its ground state, the DDCS's are found to be moderately sensitive to the choice of $\bar{I}_Z$; when H is left in the $n=2$ state, the DDCS's are found to be insensitive to the choice of $\bar{I}_Z$.

In Figs. 5 and 6 we have plotted the target-dependent parts of the two integrands in Eq. (4) on which the Galilean-invariant DDCS depends. It is the small momentum-transfer region that is most significant for the DDCS. In this region it is easily shown from the definitions of the atomic form factor and the incoherent-scattering function that

$$|\epsilon_{00}^Z(K) - Z|^2/K^3 \propto K \quad \text{for } K \to 0 , \tag{15}$$

and

$$S_{\rm inc}^Z(K)/K^3 \propto K^{-1} \quad \text{for } K \to 0 . \tag{16}$$

Because of the singularity at small K in the second integrand in Eq. (4) due to the behavior in Eq. (16), the second integral always contributes significantly to the magnitude of the DDCS's for the small values of the detached-electron momenta k_P that are of interest in this work. (For light elements, in fact, the second integral predominates over the first integral.) In addition, because of this singularity, the decrease in $K_{\min}^n(\bar{I}_Z)$ with increasing Z (shown in Table I) significantly augments the second integral in Eq. (4) as a result of the lower integration limit in a region where the integrand is large. This augmentation with increasing Z is, in addition to the expected increase in the DDCS's with increasing Z, simply due to increases in the atomic form factors and the incoherent-scattering functions. The dependences of the atomic form factor and the incoherent-scattering function on Z, for a fixed value of the momentum transfer K, are only known numerically and not analytically.[12]

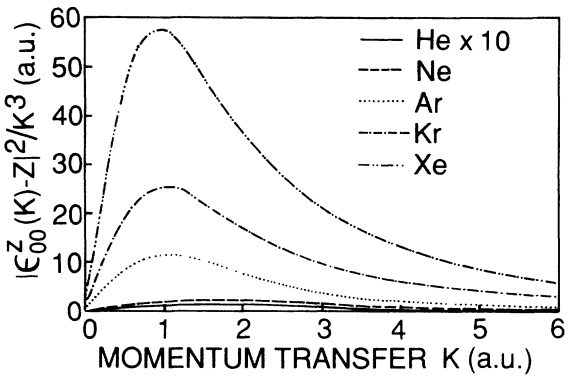

FIG. 5. Target-dependent part of the integrand of the first integral in Eq. (4) for the Galilean-invariant DDCS plotted vs momentum transfer K for five rare-gas target atoms. Values of the atomic form factor $\epsilon_{00}^Z(K)$ were obtained from the work of Hubbell *et al.* (Ref. 12).

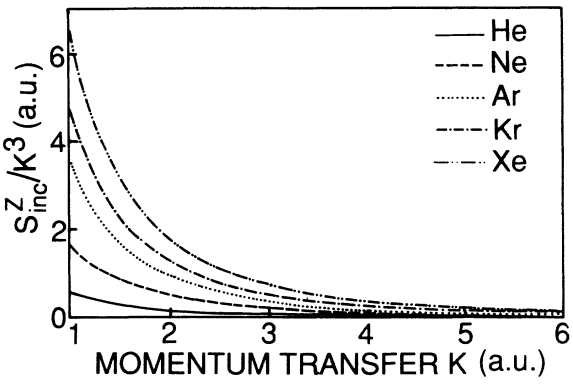

FIG. 6. Target-dependent part of the integrand of the second integral in Eq. (4) for the Galilean-invariant DDCS plotted vs momentum transfer K for five rare-gas target atoms. Because of the singularity of $S^Z_{inc}(K)/K^3$ as $K \rightarrow 0$ [cf. Eq. (16)], we plot this function only for $K \geq 1$. Values of the atomic scattering function $S^Z_{inc}(K)$ were obtained from Hubbell *et al.* (Ref. 12).

A. 0.5-MeV $H^- + T \rightarrow H(1s) + T^* + e^-$

In Fig. 7 we present our calculated Galilean-invariant DDCS's for process (1) for the rare gases He, Ne, Ar, Kr, and Xe. We observe that the DDCS for Xe is nearly two orders of magnitude larger than that for He. We observe also how the s- and p-wave interference minimum[7,10,18] that is a prominent feature in the DDCS for He (i.e., the valley extending from $k_P \approx 0.2$, $\theta_P \approx 0°$, to $k_P = 0.5$, $\theta_P \approx 140°$) has nearly disappeared for the heavier rare gases Kr and Xe. This effect has been explained by Macek, Menendez, and Duncan,[4] who argued that the s- and p-wave interference term stemming from the second integral in Eq. (4) is proportional to $K^{n=1}_{min}(\bar{I}_Z)$.[21] Now, the larger the value of $\bar{I}_Z$, the larger will be $K^{n=1}_{min}(\bar{I}_Z)$, and therefore the more prominent the interference minimum of s and p partial waves.[4] Values for $K^{n=1}_{min}(\bar{I}_Z)$ are given in Table I, which shows that $K^{n=1}_{min}(\bar{I}_Z)$ is 2.5 times larger for He than for Xe for 0.5-MeV H^- projectiles at the equal-velocity peak position.

The argument of Macek, Menendez, and Duncan[4] assumes that the target atom is left in an excited state, i.e., that the second integral in Eq. (4) predominates over the first one. This is very true for light elements but not true for heavier elements, as may be inferred from the two-orders-of-magnitude-greater value of the first integrand in Eq. (4) for Xe as compared with that for He, as shown in Fig. 5. However, the first integral in Eq. (4), corresponding to leaving the target unexcited, does not have a prominent s- and p-wave interference term. Hence it merely contributes to the "background" on which sits the target-dependent interference minimum stemming from the second integral in Eq. (4). These behaviors of the two integrals, which contribute to the Galilean-invariant DDCS defined in Eq. (4), are compared in Fig. 8 for the cases of the He and Xe targets. In Figs. 8(a) and 8(c) we see that the unexcited-target contributions to the DDCS's [stemming from the first integral in Eq. (4)] for He and Xe targets, respectively, have no detectable interference minima.[22] In Figs. 8(b) and 8(d) we see that the excited-target contributions to the DDCS's [stemming from the second integral in Eq. (4)] for He and Xe targets, respectively, have significant interference minima, with that for He much more significant than that for Xe due to the proportionality of the interference term to $K_{min}(\bar{I}_Z)$, as explained by Macek and co-workers.[4,21] The sum of the partial DDCS's in Figs. 8(a) and 8(b) for He, and in Figs. 8(c) and 8(d) for Xe, give the DDCS's shown in Figs. 7(a) and 7(e), respectively. Due to the negligible contribution of the unexcited-target state to the DDCS in the case of He, the results in Figs. 7(a) and 8(b) are the same to within a few percent. In contrast, in the case of Xe, the large contribution to the DDCS of the unexcited-target state [cf. Fig. 8(c)] tends to reduce the significance of the s- and p-wave interference stemming from the excited-target-state contribution to the DDCS [cf. Fig. 8(d)]. This is seen by comparing Fig. 7(e) with Fig. 8(d).

B. 0.5-MeV $H^- + T \rightarrow H(n=2) + T^* + e^-$

In Fig. 9 we present our results for the projectile-frame DDCS's for processes (2) for the rare-gas target atoms He, Ne, Ar, Kr, and Xe for the case of 0.5-MeV H^- projectiles. Once again we note the two-orders-of-magnitude-greater values of the DDCS for Xe targets than for He targets. We note also that the near isotropic behavior of the DDCS in the projectile frame in the case of He is atypical. The ^1P symmetry of the prominent shape resonance feature in the DDCS implies that the angular distribution should depend on both constant and $\cos^2\theta_P$ terms. As pointed out by us previously,[23] the coefficient of the $\cos^2\theta_P$ term in the case of He is anomalously small because of a near cancellation of positive and negative contributions to the relevant integral over the momentum transfer K. The other target atoms do not have such a near cancellation, and hence the dependence of the DDCS on $\cos^2\theta_P$ is clearly visible.

C. Comparisons with experimental results

Transforming our calculated results for the Galilean-invariant DDCS's for processes (1) and (2) to the laboratory frame, we can make comparison with three sets of experimental results for rare-gas targets. Figure 10 compares our calculated results with the data of Macek, Menendez, and Duncan[4] for the processes,

$$0.5\text{-MeV } H^- + T \rightarrow H^* + T^* + e^- , \tag{17}$$

for He, Ne, and Ar targets and for an electron detachment angle of $\theta_L = 0.7°$. Note, in particular, that the experimental results include contributions from all final states of the H atom. Also, the relative experimental measurements are normalized to the sum of our predicted DDCS's for $H(1s)$ and $H(n=2)$ final states at the energy of the lower-energy peak. We see that inclusion of $H(n=2)$ final states in the theoretical calculations greatly improves agreement with experiment as compared with calculations that only include $H(1s)$ final states.[19]

The higher-energy peak in the laboratory-frame DDCS is due to the $^1P°$ shape resonance feature in the DDCS's

for H($n=2$) final states. We have shown elsewhere[2] that this feature in the DDCS decreases very rapidly with increasing angle θ_L in the forward direction. Consequently, we expect that the occurrence of experimentally measured higher-energy peaks, which are lower in magnitude and broader in energy than the theoretical predictions at $\theta_L=0.7°$, has much to do with the large angular acceptance ($\pm 0.4°$) in these measurements.[4]

Figure 11 compares our calculated DDCS results with data of Duncan and Menendez[5] for the process,

$$0.5\text{-MeV } H^- + Ar \rightarrow H^* + Ar^* + e^- , \tag{18}$$

for the three electron-detachment angles $\theta_L=0.8°$, 1.3°, and 3.8°. For both $\theta_L=0.8°$ and 1.3°, the relative experimental measurements are normalized to our theoretical predictions at the energy position of the lower-energy peak. For $\theta_L=3.8°$, the experimental results are normalized to our calculations at the energy position of the peak in the DDCS. At these larger detection angles θ_L, the decrease with angle of the $^1P^\circ$ resonance feature is less

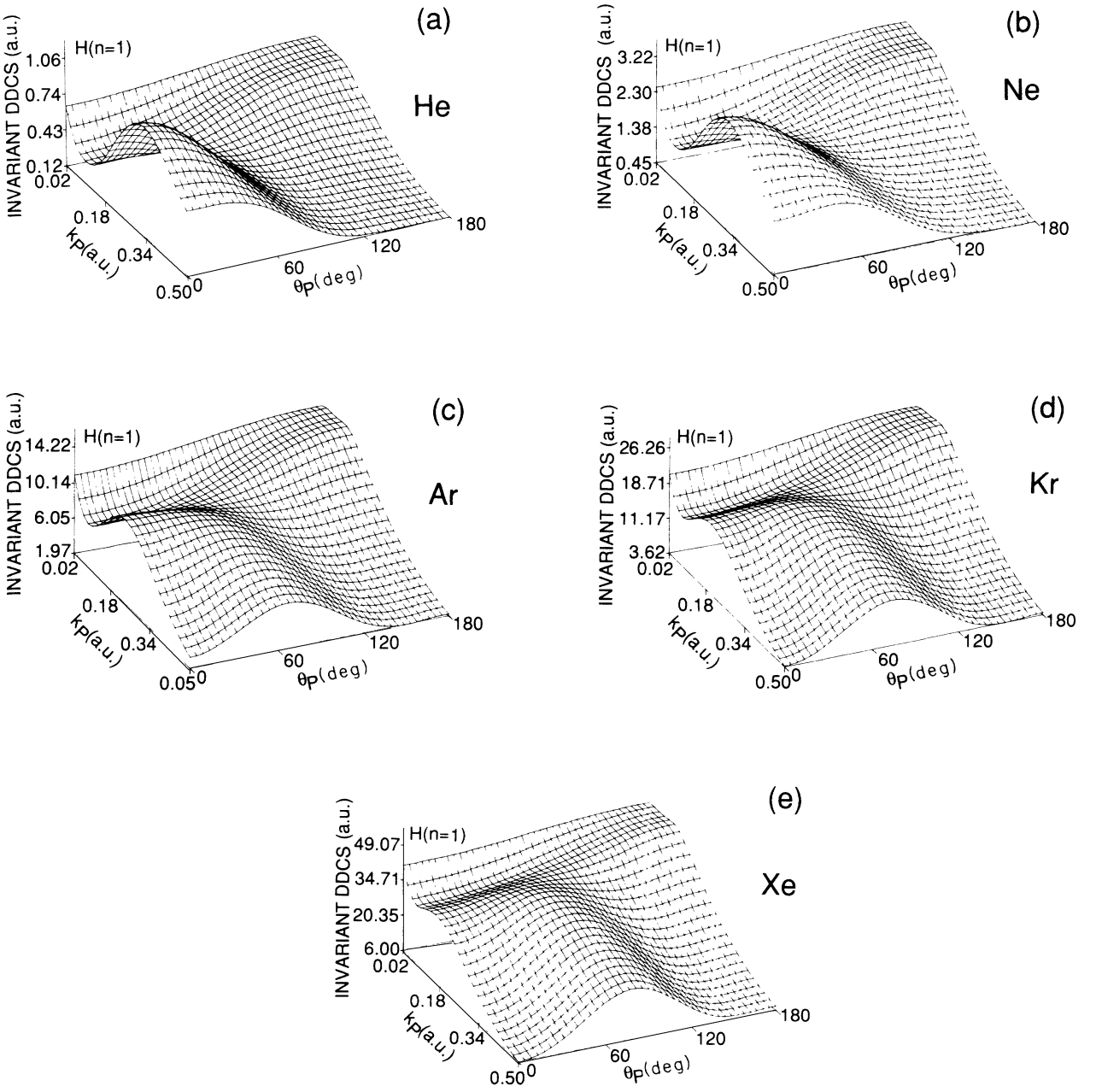

FIG. 7. Galilean-invariant DDCS's calculated according to Eq. (4) for the processes 0.5-MeV $H^- + T \rightarrow H(1s) + T^* + e^-$ plotted vs electron momentum $\mathbf{k}_P \equiv (k_P, \theta_P)$ in the projectile (P) frame. The target atoms T are (a) He, (b) Ne, (c) Ar, (d) Kr, and (e) Xe.

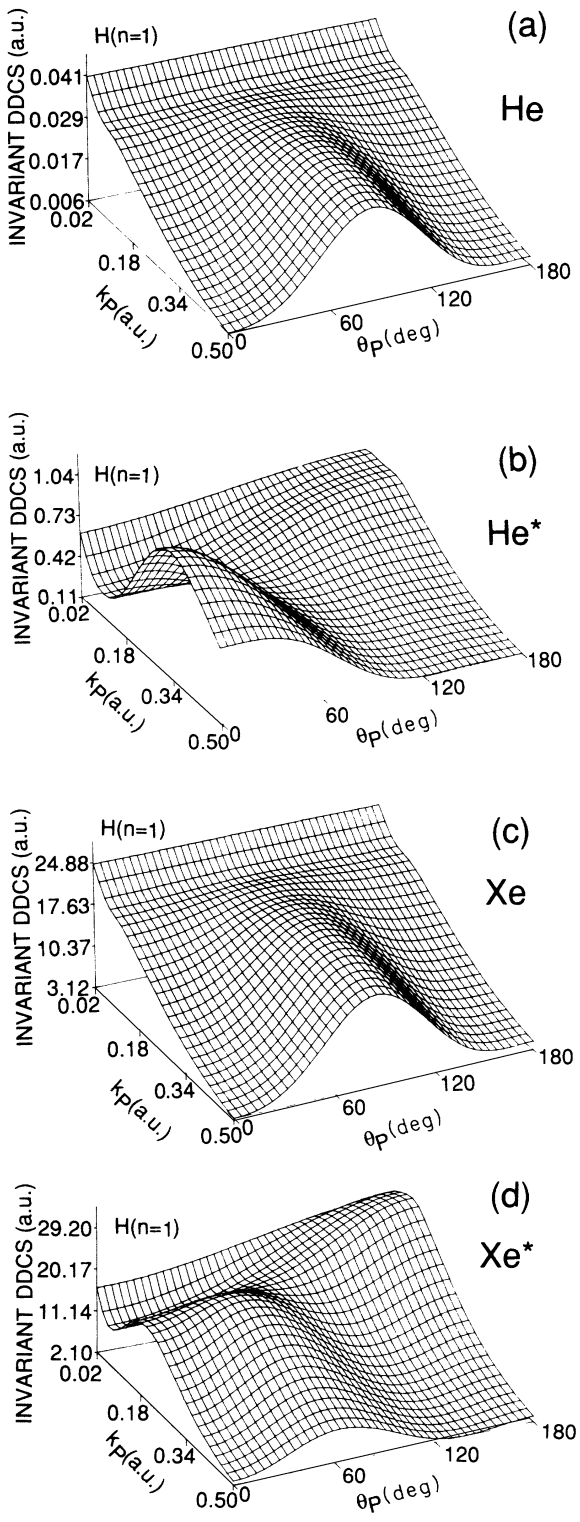

FIG. 8. Contributions of the unexcited-target final state [calculated from the first integral in Eq. (4)] and excited-target final states [calculated from the second integral in Eq. (4)] to the Galilean-invariant DDCS's for the processes 0.5-MeV $H^- + T \rightarrow H(1s) + T^* + e^-$ for He and Xe targets. The partial DDCS's are plotted vs electron momentum $\mathbf{k}_P \equiv (k_P, \theta_P)$ in the projectile (P) frame. (a) unexcited He final state; (b) excited He final states; (c) unexcited Xe final state; (d) excited Xe final states.

rapid than at smaller angles. Hence, the discrepancies between theoretical and experimental results stemming from the experimental angular resolution are significantly less noticeable than those for the $\theta_L = 0.7°$ data shown in Fig. 10. Thus, for $\theta_L = 0.8°$, one sees that the experimental higher-energy peak is lower in magnitude and broader in energy than the theoretically predicted peak. However, for both $\theta_L = 1.3°$ and $\theta_L = 3.8°$, theory and experiment are in quite good agreement.

Finally, in Fig. 12 we compare our calculated DDCS results with the data of Andersen, Bangsgaard, and Sørensen[6] for the process,

$$0.1\text{-MeV } H^- + Xe \rightarrow H(n=2) + Xe^* + e^- . \quad (19)$$

The experimental data are for $\theta_L = 0°$, but the angular acceptance is 0.506°. For this reason, we show in Fig. 12(a) our theoretical predictions for the angles $\theta_L = 0.0°$, 0.1°, 0.2°, and 0.3°. The cusp feature[1,2] at the equal-velocity position is most prominent for these low angles, but decreases rapidly with increasing angle θ_L. The shoulder features[1,2] at these low angles are due to the $^1P°$-shape resonance in the projectile-frame DDCS. The experimental data show a marked difference in the peak heights of these two shoulder features, which is not reproduced in our calculations. Nevertheless, the overall qualitative agreement of theory and experiment is quite reasonable.

V. DISCUSSION AND CONCLUSIONS

In this work we have extended our previous studies[1,2] of the DDCS's for 0.5-MeV H^- detachment collisions with He targets by examining the dependence of the DDCS's on both the projectile energy and the target atom. For any target, the most interesting and significant features of the DDCS occur in the projectile frame for low values of the electron momentum k_P. Understanding the projectile-energy dependence of the laboratory-frame DDCS is thus a matter of examining the kinematics of the transformation of the projectile-frame results (or, more precisely, the Galilean-invariant results) to the laboratory frame, as we have done in Sec. III.

The target dependence of the DDCS's is a more complex problem. Generally speaking, the larger the atomic number of the target atom, the larger the DDCS's. However, this dependence has many detailed aspects. Thus, for He targets, we have shown that the contribution of unexcited He final states to the DDCS is negligible compared with the contributions of excited He final states. On the other hand, for Xe targets, both unexcited and excited Xe final states contribute significantly to the DDCS. The prominence of the s- and p-wave interference in the DDCS for $H(1s)$ final states decreases with increasing atomic number (for the rare-gas targets considered in this work, at least) because of the decreasing average excitation energy of these targets as the atomic number in-

creases, as first pointed out by Macek, Menendez, and Duncan.[4] Our earlier prediction,[23] that the isotropic behavior of the H($n=2$) projectile-frame DDCS is anomalous for the case of 0.5-MeV H^- detachment collisions with He targets, has been confirmed here. We find that for the other rare-gas targets (as well as for other incident projectile energies), the H($n=2$) DDCS's show the expected dependence on $\cos^2\theta_P$ in the projectile frame.

In comparison with experimental results, we find that inclusion of H($n=2$) excited final states in the theoretical

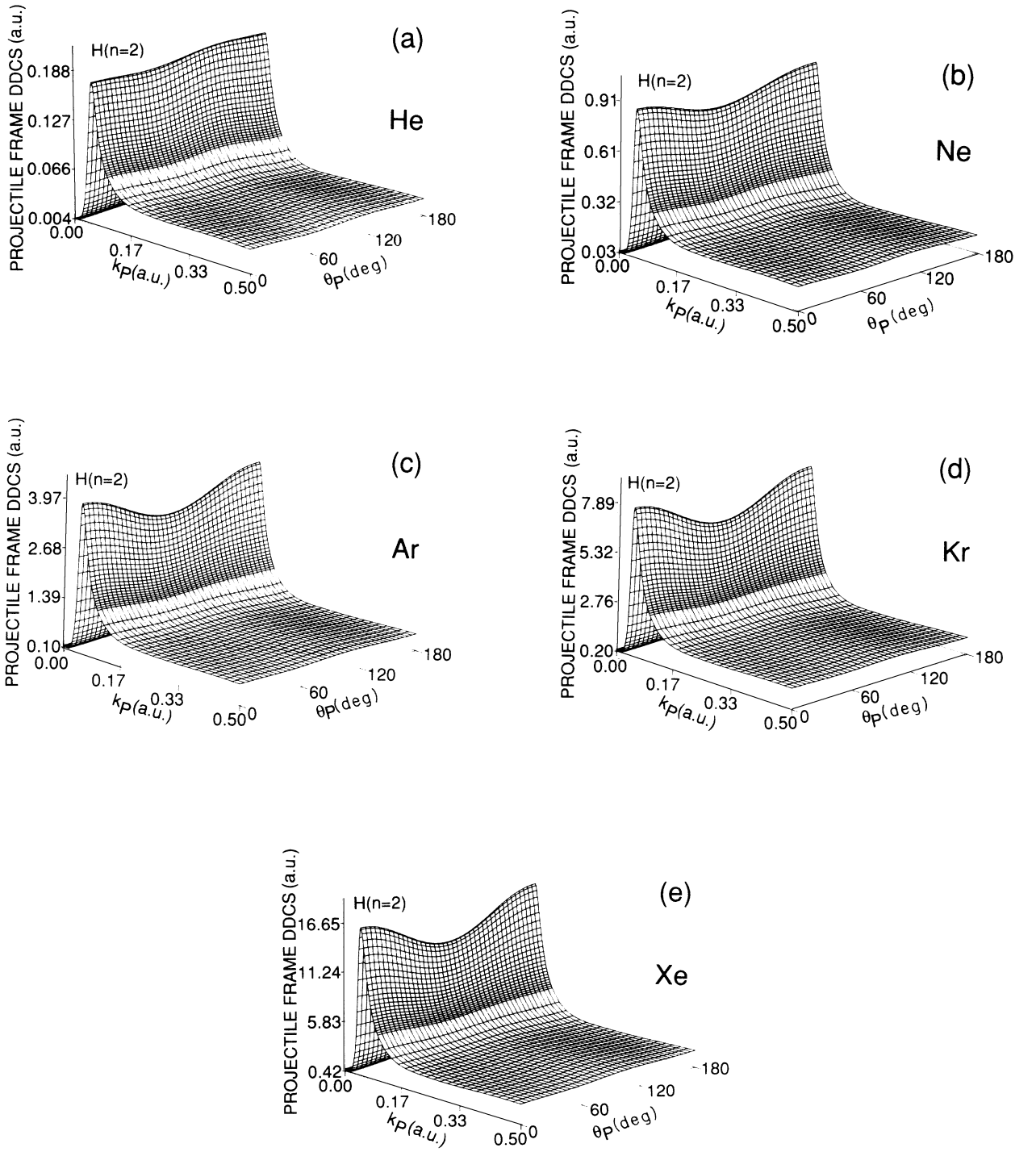

FIG. 9. Projectile-frame DDCS's calculated according to Eq. (4) for the processes 0.5-MeV $H^- + T \rightarrow H(n=2) + T^* + e^-$ plotted vs electron momentum $\mathbf{k}_P \equiv (k_P, \theta_P)$ in the projectile (P) frame. The target atoms T are (a) He, (b) Ne, (c) Ar, (d) Kr, and (e) Xe.

calculations, in addition to unexcited H(1s) final states, greatly improves agreement with the experimental measurements[4,5] that do not measure the final state of the H atom. Our results for 0.1-MeV H^- collisions with Xe targets resulting in H($n=2$) final states are in qualitative agreement with experimental results;[6] in particular, the cusp and shape resonance features found experimentally are reproduced qualitatively in our calculations. In all such comparisons, as we have noted before,[1,2] the most prominent features are very sensitive functions of the electron-detachment angle. Hence, the generally large experimental acceptance angles make precise comparison of theory and experiment difficult without a convolution of the theoretical results using experimental angular and energy convolution functions. In the one case where we have been able to carry out such convolutions, agreement between the results of theory and experiment is excellent.[24]

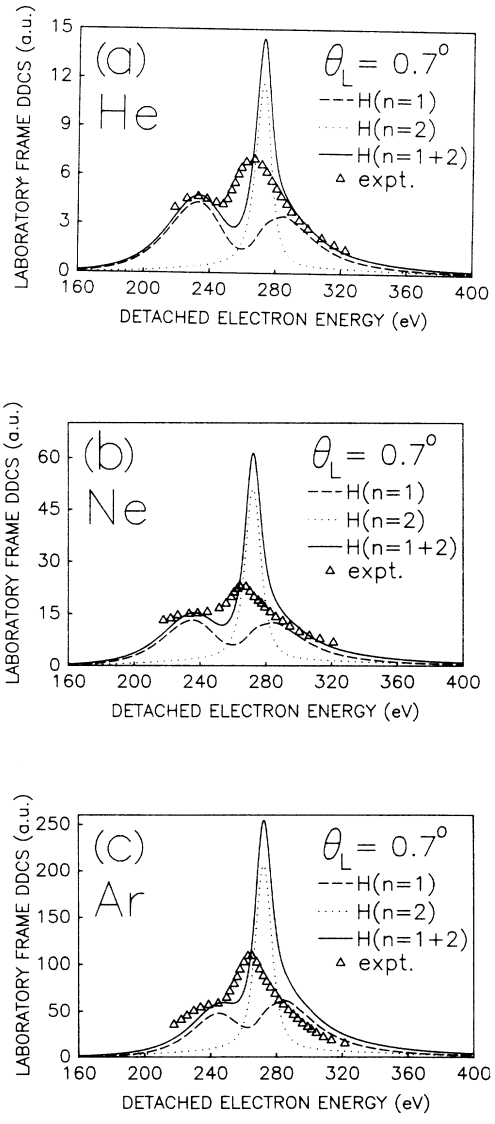

FIG. 10. Laboratory-frame DDCS's for the process 0.5-MeV $H^- + T \rightarrow H^* + T^* + e^-$ for electron detachment at $\theta_P = 0.7°$. Dashed curves, present theoretical results for H($n=1$) final states; dotted curves, present theoretical results for H($n=2$) final states; solid curves, sum of present theoretical results for H($n=1$) and H($n=2$) final states; triangles, experimental results of Macek, Menendez, and Duncan (from Ref. 4), normalized to our solid curves at the position of the lower-energy peak. (a) He targets; (b) Ne targets; (c) Ar targets.

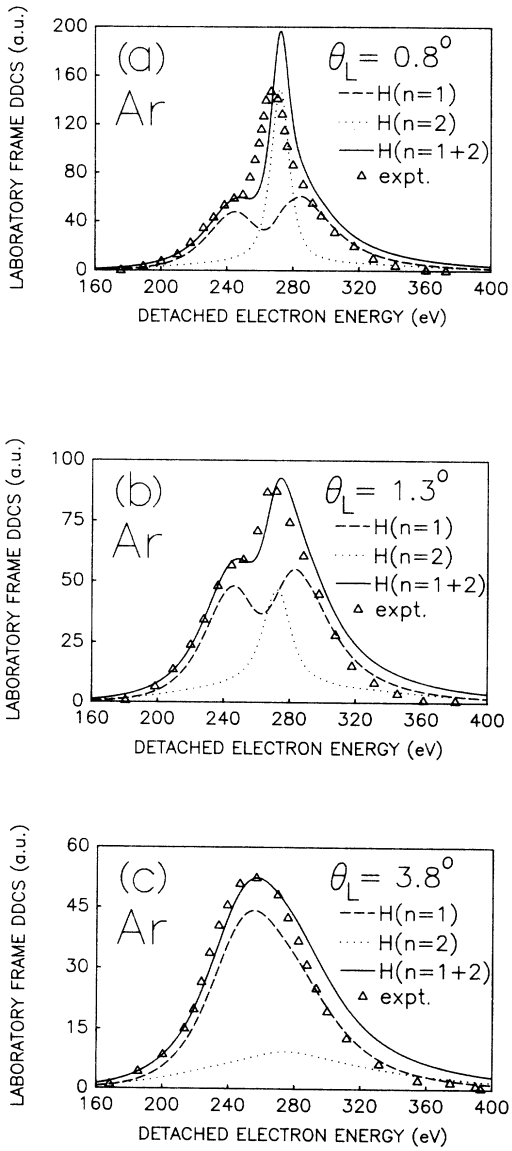

FIG. 11. Laboratory-frame DDCS's for the process 0.5-MeV $H^- + Ar \rightarrow H^* + Ar^* + e^-$ for electron-detachment angles of (a) $\theta_L = 0.8°$, (b) $\theta_L = 1.3°$, and (c) $\theta_L = 3.8°$. Solid, dashed, and dotted curves are defined as in Fig. 10. Triangles, experimental results of Duncan and Menendez (Ref. 5), normalized to our solid curves at the position of the lower-energy peak for $\theta_L = 0.8°$ and 1.3° and at the position of the single peak for $\theta_L = 3.8°$.

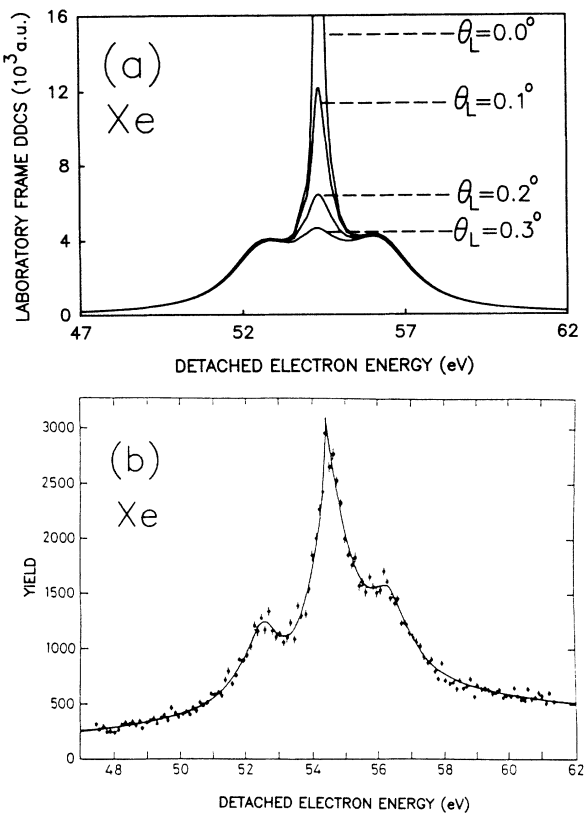

FIG. 12. Laboratory-frame DDCS's for the process 0.1-MeV $H^- + Xe \rightarrow H(n=2) + Xe^* + e^-$. (a) Present theoretical results for electron detachment angles $\theta_L = 0.0°$, 0.1°, 0.2°, and 0.3°. (b) Experimental results of Andersen, Bangsgaard, and Sørensen (from Ref. 6) for $\theta_L = 0.0°$. The experimental angular acceptance is 0.506°.

Finally, we note that our present and previous[1,2,7] studies of the DDCS's for H^--detachment collisions on rare-gas targets have relevance to current interest in electron-correlation effects on heavy-particle collision processes.[25-28] In particular, our analysis of the separate contributions to the DDCS's of unexcited- and excited-target states (cf. Fig. 8 and its discussion in Sec. IV A above) corresponds to the "screening-antiscreening" effects discussed by McGuire and co-workers,[25,28] to the "two-center correlations" discussed by Stolterfoht,[27] and, of course, to the pioneering studies of Bates and Griffing[29] on inelastic effects in hydrogen-atom collision processes. Detailed experimental confirmation of such electron-correlation effects on total cross sections have recently been reported.[26] Our studies contribute to the knowledge of such correlation effects on differential cross sections.

ACKNOWLEDGMENTS

One of us (C.R.L.) gratefully acknowledges the hospitality of Dr. Keh-Ning Huang and Dr. Tsin-Fu Jiang at the Institute of Atomic and Molecular Sciences of the Academia Sinica in Taiwan, Republic of China, where many of the calculations reported here were carried out. We thank Dr. L. H. Andersen, Dr. M. M. Duncan, and Dr. M. G. Menendez for providing us with details of their experimental measurements. This work was supported, in part, by the U.S. Department of Energy, Office of Basic Energy Sciences, Division of Chemical Sciences, under Grant No. DE-FG02-88ER13955.

*Present address: Department of Radiation Oncology and Nuclear Medicine, Thomas Jefferson University Hospital, Philadelphia PA 19107.

[1]C. R. Liu and A. F. Starace, Phys. Rev. Lett. **62**, 407 (1989).

[2]C. R. Liu and A. F. Starace, Phys. Rev. A **40**, 4926 (1989), and references therein to prior work.

[3]M. G. Menendez and M. M. Duncan, Phys. Rev. A **20**, 2327 (1979).

[4]J. Macek, M. G. Menendez, and M. M. Duncan, Phys. Rev. A **29**, 516 (1984).

[5]M. M. Duncan and M. G. Menendez, Phys. Rev. A **16**, 1799 (1977).

[6]L. H. Andersen, J. P. Bangsgaard, and J. Sørensen, Phys. Rev. Lett. **57**, 1558 (1986).

[7]C. H. Park, A. F. Starace, and J. Macek, Phys. Rev. A **31**, 1336 (1985).

[8]We note here several misprints in Refs. 1 and 2. In both Eq. (3) of Ref. 1 and Eq. (16) of Ref. 2, the sign of the term $+1/n^2$ should be changed to $-1/n^2$. In Ref. 2, the last factor X in Eq. (34) should be replaced by $X^\dagger$, in Eq. (38) the entry $\bar{l}$ in the $3j$ symbol should be replaced by $\bar{l}'$, and, in the Appendix of Ref. 2, the superscripts for Refs. 43 and 46 should be interchanged.

[9]Cf. Ref. 7, Eq. (12).

[10]N. Maleki and J. H. Macek, Phys. Rev. A **26**, 3198 (1982).

[11]Cf. Ref. 7, Sec. III A.

[12]J. H. Hubbell, W. J. Veigele, E. A. Briggs, R. T. Brown, D. T. Cromer, and R. J. Howerton, J. Phys. Chem. Ref. Data **4**, 471 (1975).

[13]F. Drepper and J. S. Briggs, J. Phys. B **9**, 2063 (1976).

[14]See discussion in Ref. 2, Sec. II B.

[15]J. Macek, J. Phys. B **1**, 831 (1968).

[16]U. Fano, Rep. Prog. Phys. **46**, 97 (1983).

[17]A. F. Starace, in *Fundamental Processes of Atomic Dynamics*, edited by J. S. Briggs, H. Kleinpoppen, and H. O. Lutz (Plenum, New York, 1988), pp. 235–258.

[18]M. R. Frantz, L. A. Wright, and T. C. Genoni, Phys. Rev. A **24**, 1135 (1981).

[19]Note that in transforming the $H(n=2)$ DDCS from the projectile frame to the laboratory frame, we have shifted the $^1P^\circ$-shape resonance peak to lie 18.9 meV lower in energy in the projectile frame, in order to place it at the position known from the photodetachment experiments of (a) H. C. Bryant, B. D. Dieterle, J. Donahue, H. Sharifian, H. Tootoonchi, D. M. Wolfe, P. A. M. Gram, and M. A. Yates-Williams, Phys. Rev. Lett. **38**, 228 (1977); (b) H. C. Bryant, D. A. Clark, K. B. Butterfield, C. A. Frost, H. Sharifian, H. Tootoonchi, J. B. Donahue, P. A. M. Gram, M. E. Hamm, R. W. Hamm, J. C. Pratt, M. A. Yates, and W. W. Smith, Phys. Rev. A **27**, 2889 (1983).

[20]J. A. R. Samson, Adv. At. Mol. Phys. **2**, 177 (1966), Fig. 16.

[21]This proportionality may be also understood from Eqs. (40)–(42) of Ref. 2. For the $H(1s)$ final state, the s- and p-wave interference term corresponds to $\Lambda = 1$ in the sum in Eq.

(41). But the factor $P_{\Lambda=1}(\zeta)$ equals ζ, which is approximately equal to $K/2k_i + K_{\min}/K$. To the extent that small values of K predominate in calculating the integrals over K in Eq. (42) for the DDCS, $K_{\min}/K \gg K/2k_i$, and hence the interference term is proportional to $K_{\min}$.

[22]This absence of a detectable interference minimum stemming from the first integral in Eq. (4) may be explained in part by the proportionality of its interference term to $K_{\min}(0)$ (cf. Ref. 21). For 0.5-MeV incident H^- projectiles, $K_{\min}(0) = 6.3 \times 10^{-3}$ a.u. This contrasts to the proportionality of the interference term stemming from the second integral in Eq. (4) to $K_{\min}(\bar{I}_Z)$. For He, $K_{\min}(\bar{I}_{He}) = 2.9 \times 10^{-1}$ a.u., while for Xe, $K_{\min}(\bar{I}_{Xe}) = 1.2 \times 10^{-1}$ a.u. (cf. Table I). On these grounds alone, then, the interference terms stemming from the second integral in Eq. (4) should be one to two orders of magnitude larger than those stemming from the first integral in Eq. (4).

[23]Cf. Ref. 2, Sec. III B.

[24]Cf. Ref. 2, Fig. 6.

[25]J. H. McGuire, N. Stolterfoht, and P. R. Simony, Phys. Rev. A **24**, 97 (1981).

[26]H. P. Hülskötter, W. E. Meyerhof, E. Dillard, and N. Guardala, Phys. Rev. Lett. **63**, 1938 (1989).

[27]N. Stolterhoft, in *Proceedings of the Conference on Spectroscopy and Collisions of Few-Electron Ions, Bucharest, 1988,* edited by V. Florescu and V. Zoran (World Scientific, Singapore, 1989), p. 342; Phys. Scr. (to be published).

[28]J. H. McGuire and J. C. Stratton, in *Proceedings of the 16th International Conference on the Physics of Electronic and Atomic Collisions, New York, 1989,* AIP Conf. Proc. No. 205, edited by A. Dalgarno, R. S. Freund, P. M. Koch, M. S. Lubell, and T. B. Lucatorto (AIP, New York, 1990), pp. 280–289.

[29]D. R. Bates and G. Griffing, Proc. Phys. Soc. **66**, 961 (1953); **67**, 663 (1954); **68**, 90 (1955).